DMD-based software-configurable spatially-offset Raman spectroscopy for spectral depth-profiling of optically turbid samples

Zhiyu Liao,[1] Faris Sinjab,[1] Graham Gibson,[2] Miles Padgett,[2] and Ioan Notingher[1,*]

[1]*School of Physics and Astronomy, University Park, University of Nottingham, Nottingham, NG7 2RD, UK*
[2]*School of Physics and Astronomy, University of Glasgow, Kelvin Building, Glasgow G12 8QQ, UK*
**Ioan.Notingher@nottingham.ac.uk*

Abstract: Spectral depth-profiling of optically turbid samples is of high interest to a broad range of applications. We present a method for measuring spatially-offset Raman spectroscopy (SORS) over a range of length scales by incorporating a digital micro-mirror device (DMD) into a sample-conjugate plane in the detection optical path. The DMD can be arbitrarily programmed to collect/reject light at spatial positions in the 2D sample-conjugate plane, allowing spatially offset Raman measurements. We demonstrate several detection geometries, including annular and simultaneous multi-offset modalities, for both macro- and micro-SORS measurements, all on the same instrument. Compared to other SORS modalities, DMD-based SORS provides more flexibility with only minimal additional experimental complexity for subsurface Raman collection.

OCIS codes: (230.0230) Optical devices; (170.5660) Raman spectroscopy.

References and links

1. S. Ekgasit and H. Ishida, "New optical depth-profiling technique by use of the multiple-frequency approach with single ATR FT-IR spectrum: theoretical development," Appl. Spectrosc. **51**(10), 1488–1495 (1997).
2. M. W. Urban, C. L. Allison, G. L. Johnson, and F. Di Stefano, "Stratification of butyl acrylate/polyurethane (BA/PUR) latexes: ATR and step-scan photoacoustic studies," Appl. Spectrosc. **53**(12), 1520–1527 (1999).
3. R. W. Jones and J. F. McClelland, "Quantitative depth profiling using saturation-equalized photoacoustic spectra," Appl. Spectrosc. **56**(4), 409–418 (2002).
4. W. Faubel, S. Heissler, and R. A. Palmer, "Quantitative analysis of corroded copper patina by step scan and rapid scan photoacoustic Fourier transform infrared spectroscopy," Rev. Sci. Instrum. **74**(1), 331–333 (2003).
5. I. Notingher, R. E. Imhof, P. Xiao, and F. C. Pascut, "Spectral depth profiling of arbitrary surfaces by thermal emission decay-Fourier transform infrared spectroscopy," Appl. Spectrosc. **57**(12), 1494–1501 (2003).
6. I. Notingher and R. E. Imhof, "Mid-infrared in vivo depth-profiling of topical chemicals on skin," Skin Res. Technol. **10**(2), 113–121 (2004).
7. N. J. Everall, "Modeling and measuring the effect of refraction on the depth resolution of confocal Raman microscopy," Appl. Spectrosc. **54**(6), 773–782 (2000).
8. N. J. Everall, "Confocal Raman microscopy: why the depth resolution and spatial accuracy can be much worse than you think," Appl. Spectrosc. **54**(10), 1515–1520 (2000).
9. P. J. Caspers, G. W. Lucassen, E. A. Carter, H. A. Bruining, and G. J. Puppels, "In vivo confocal Raman microspectroscopy of the skin: noninvasive determination of molecular concentration profiles," J. Invest. Dermatol. **116**(3), 434–442 (2001).
10. P. Matousek, I. P. Clark, E. R. C. Draper, M. D. Morris, A. E. Goodship, N. Everall, M. Towrie, W. F. Finney, and A. W. Parker, "Subsurface probing in diffusely scattering media using spatially offset Raman spectroscopy," Appl. Spectrosc. **59**(4), 393–400 (2005).
11. Cobalt, Airport security. www.cobaltlight.com/security/ (Accessed February 2016)
12. C. Eliasson, N. A. Macleod, and P. Matousek, "Noninvasive detection of concealed liquid explosives using Raman spectroscopy," Anal. Chem. **79**(21), 8185–8189 (2007).
13. C. Eliasson and P. Matousek, "Noninvasive authentication of pharmaceutical products through packaging using spatially offset Raman spectroscopy," Anal. Chem. **79**(4), 1696–1701 (2007).

#260530 Received 7 Mar 2016; revised 14 Apr 2016; accepted 20 Apr 2016; published 1 Jun 2016

14. W. J. Olds, E. Jaatinen, P. Fredericks, B. Cletus, H. Panayiotou, and E. L. Izake, "Spatially offset Raman spectroscopy (SORS) for the analysis and detection of packaged pharmaceuticals and concealed drugs," Forensic Sci. Int. **212**(1-3), 69–77 (2011).
15. M. Bloomfield, D. Andrews, P. Loeffen, C. Tombling, T. York, and P. Matousek, "Non-invasive identification of incoming raw pharmaceutical materials using Spatially Offset Raman Spectroscopy," J. Pharm. Biomed. Anal. **76**, 65–69 (2013).
16. B. Sharma, K. Ma, M. R. Glucksberg, and R. P. Van Duyne, "Seeing through bone with surface-enhanced spatially offset Raman spectroscopy," J. Am. Chem. Soc. **135**(46), 17290–17293 (2013).
17. J.-L. H. Demers, F. W. L. Esmonde-White, K. A. Esmonde-White, M. D. Morris, and B. W. Pogue, "Next-generation Raman tomography instrument for non-invasive in vivo bone imaging," Biomed. Opt. Express **6**(3), 793–806 (2015).
18. P. Matousek and N. Stone, "Development of deep subsurface Raman spectroscopy for medical diagnosis and disease monitoring," Chem. Soc. Rev. **45**(7), 1794–1802 (2016).
19. M. D. Keller, E. Vargis, N. de Matos Granja, R. H. Wilson, M. A. Mycek, M. C. Kelley, and A. Mahadevan-Jansen, "Development of a spatially offset Raman spectroscopy probe for breast tumor surgical margin evaluation," J. Biomed. Opt. **16**(7), 077006 (2011).
20. D. T. Yang and Y. B. Ying, "Applications of Raman spectroscopy in agricultural products and food analysis: a review," Appl. Spectrosc. Rev. **46**(7), 539–560 (2011).
21. C. Eliasson, N. A. Macleod, and P. Matousek, "Non-invasive detection of cocaine dissolved in beverages using displaced Raman spectroscopy," Anal. Chim. Acta **607**(1), 50–53 (2008).
22. P. Matousek, "Inverse spatially offset Raman spectroscopy for deep noninvasive probing of turbid media," Appl. Spectrosc. **60**(11), 1341–1347 (2006).
23. Z. Wang, H. Ding, G. Lu, and X. Bi, "Use of a mechanical iris-based fiber optic probe for spatially offset Raman spectroscopy," Opt. Lett. **39**(13), 3790–3793 (2014).
24. J. Qin, M. S. Kim, W. F. Schmidt, B.-K. Cho, Y. Peng, and K. Chao, "A line-scan hyperspectral Raman system for spatially offset Raman spectroscopy," J. Raman Spectrosc. **47**(4), 437–443 (2016).
25. G. M. Gibson, M. Dienerowitz, P. A. Kelleher, A. R. Harvey, and M. J. Padgett, "A multi-object spectral imaging instrument," J. Opt. **15**(8), 085302 (2013).
26. P. Matousek, E. R. C. Draper, A. E. Goodship, I. P. Clark, K. L. Ronayne, and A. W. Parker, "Noninvasive Raman spectroscopy of human tissue in vivo," Appl. Spectrosc. **60**(7), 758–763 (2006).
27. C. Conti, M. Realini, C. Colombo, K. Sowoidnich, N. K. Afseth, M. Bertasa, A. Botteon, and P. Matousek, "Noninvasive analysis of thin turbid layers using microscale spatially offset Raman spectroscopy," Anal. Chem. **87**(11), 5810–5815 (2015).
28. C. Conti, C. Colombo, M. Realini, and P. Matousek, "Subsurface analysis of painted sculptures and plasters using micrometre-scale spatially offset Raman spectroscopy (micro-SORS)," J. Raman Spectrosc. **46**(5), 476–482 (2015).
29. C. Conti, M. Realini, C. Colombo, A. Botteon, and P. Matousek, "Contrasting confocal with defocusing microscale spatially offset Raman spectroscopy," J. Raman Spectrosc. in press.
30. C. Conti, M. Realini, C. Colombo, and P. Matousek, "Comparison of key modalities of micro-scale spatially offset Raman spectroscopy," Analyst (Lond.) **140**(24), 8127–8133 (2015).

1. Introduction

Non-invasive chemical depth-profiling of materials is of high interest in a broad variety of applications. A range of vibrational spectroscopy techniques has been developed for this purpose, including infrared and Raman spectroscopy. Infrared spectroscopy techniques, such as attenuated total reflectance infrared spectroscopy (ATR) [1,2], photoacoustic Fourier transform infrared (FT-IR) spectroscopy [3,4] and thermal emission decay–Fourier transform infrared spectroscopy (TED-FTIR) [5,6] offer depth discrimination in the 0.1-100 μm range. For transparent samples, confocal Raman micro-spectroscopy allows chemical depth-profiling with micrometric resolution for depths up to ~100 μm [7–9]. Spatial offset Raman spectroscopy (SORS) is an emerging technique for measuring the subsurface chemical information in diffusely scattering samples, typically from depths of 20 μm – 5 mm range, which is beyond the reach of the above mentioned techniques. Since the first demonstration in 2005 [10], SORS has found many applications in different fields, such as security screening [11,12], quality control of pharmaceutical products [13–15], non-invasive medical diagnosis [16–19] and food quality inspection [20,21]. Variants of SORS have been developed to allow measurements on samples at different scales of subsurface depth. Depending on the range of spatial offset, SORS can roughly be divided into two modalities: macro-scale SORS (macro-SORS) and micro-scale SORS (micro-SORS). The accessible depth of the former technique is in the range of 1-5 mm, while micro-SORS provides a higher depth resolution in the range of

#260530 Received 7 Mar 2016; revised 14 Apr 2016; accepted 20 Apr 2016; published 1 Jun 2016

20-1000 μm. The most common method for implementing macro-SORS measurements is using fibre optics bundles. In this configuration, optical fibres arranged in one or more concentric circles are used for the collection of the Raman spectra, where the spatial offsets are determined by the radii of the circles. While this implementation offers important advantages related to simplicity and stability, it can also impose limitations for certain applications. One such limitation is the lack of flexibility in changing the spatial offsets, thus limiting the range of sampling depths. The emergence of inverse SORS allows some flexibility in changing the spatial offsets, by delivering the laser beam in the shape of a ring and collecting the Raman photons through the optical fibres at the centre of the probe [17,22]. Inverse SORS provides more control over the number of spatial offsets, and has become a popular technique for macro-SORS measurements [22]. Wang et al. proposed a new probe design to achieve adjustable spatial offsets, where the excitation fibre was fixed at the centre of a mechanical iris, and the collection fibres were movable with the blades of the iris [23]. Nevertheless, the additional optical elements required for setting the offset distances for these techniques can complicate the probe design, require movable mechanical parts, and are not compatible for implementation into micro-SORS instruments. A simple line-scan SORS method has been recently reported that provides simultaneous SORS over a continuous range of offsets, but provides significantly lower collection efficiency for the Raman spectra [24].

In this study, we propose a simple, novel design to implement SORS by using a digital micro-mirror device (DMD) added to a conventional Raman spectrometer. Here, the instrument is based on an optical microscope to allow both micro- and macro-SORS measurements. The system enables efficient and flexible collection of SORS signals, with software-configurable selection of the spatial offsets, as well as allowing simultaneous measurements for multiple offset values. DMDs have been successfully demonstrated for multi-object fluorescence spectroscopy [25]. In this paper we demonstrate the versatility of the DMD as a software-configurable pattern of reflective pseudo-slits in various SORS collection schemes, such as concentric-rings and simultaneous multiple offsets, which can be readily realised simply by modifying the patterns displayed on the DMD. In addition, we show that the system can function as a macro- or micro-SORS instrument by simply selecting the magnification of the microscope objective or lens.

2. Materials and methods

SORS spectrometer using a DMD as the offset controller

A schematic description of the SORS instrument is presented in Fig. 1. The excitation part of the system is no different from a conventional backscattering Raman instrument. The beam of a 532 nm CW laser (Roithner LaserTechnik GmbH, RTLMSL-532, maximum power of ~20 mW) was directed via an inverted microscope (Olympus IX-71) and focused onto the sample by a microscope objective. To demonstrate the capability of the system for macro- and micro-SORS, two objective lenses were used: 2 × /0.06 NA (Olympus, Plan N) and 20 × /0.5 NA (Olympus, UPlanFL N). The laser power at the sample was ~14 mW. The Raman photons were collected by the same objective, and focused by a lens (focal length 200 mm) onto a DMD (Texas Instruments, 0.45 WVGA chipset). The DMD was actuated by a DLP® LightCrafter 4500 development module from Texas Instruments, which was modified to remove projection optics in front of the DMD. This was connected to a PC using mini HDMI connection, and controlled by a home-built LabVIEW program using the Vision Development module (National instruments). The DMD consisted of a 912 × 1140 array of individually addressable micro-mirrors (7.6 × 7.6 μm^2). The individual micro-mirrors can be switched to one of two states, 'on' and 'off', corresponding to a tilt of ± 12°. If a binary image is displayed to the DMD, it can serve as a reflective spatial filter, allowing light at arbitrary spatial positions to be reflected in one direction (say, + 12°), whilst the remaining light is rejected (−12°). The DMD was placed in the collection path of the Raman spectrometer at a

#260530 Received 7 Mar 2016; revised 14 Apr 2016; accepted 20 Apr 2016; published 1 Jun 2016

sample-conjugate plane, serving as the offset controller for SORS, as well as a slit/pinhole for the spectrometer. An inspection camera was also used to visualize patterns set on the DMD by imaging the rejected light.

The Raman photons reflected by the DMD were collected by another lens (focal length of 100 mm), passed through a notch filter (NF01-532U-25, Semrock) and then focused again in the spectrometer slit plane using a lens with focal length of 60 mm (the actual mechanical slit of the spectrometer was fully open). The detection module consisted of a spectrograph (Shamrock 303i, Andor technologies, UK) equipped with an 1800 grooves/mm grating and a thermoelectrically cooled Raman CCD camera (iDus401, Andor technologies, UK).

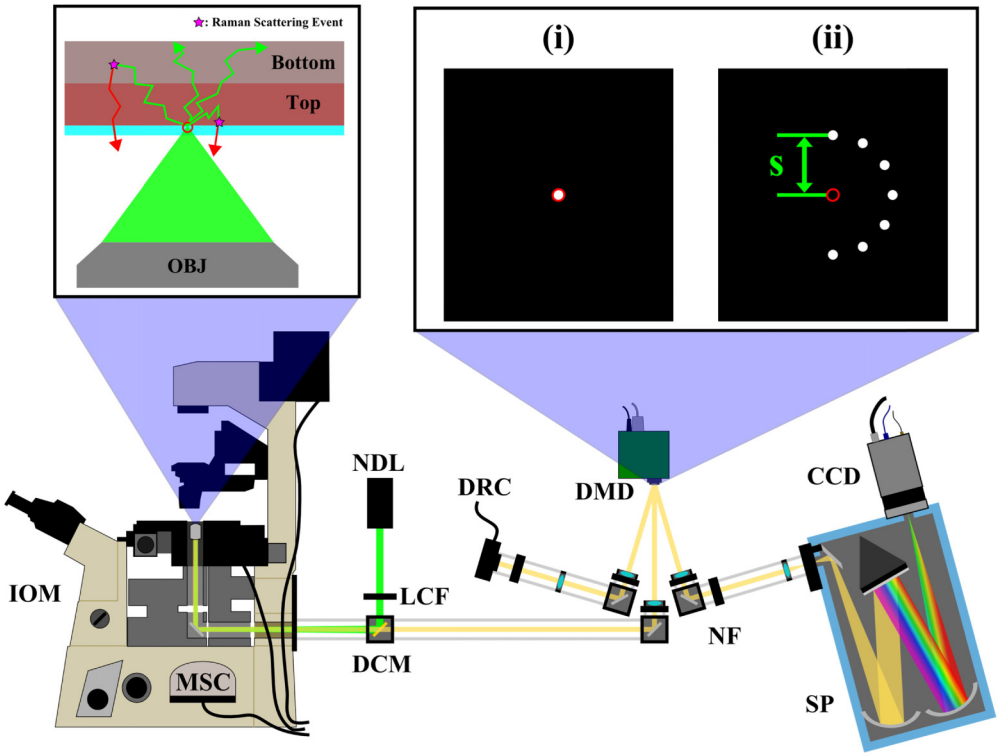

Fig. 1. Schematic of the DMD-based SORS instrument. Abbreviations: OBJ, objective; IOM, inverted optical microscope; MSC, microscope side-port camera; DCM, dichroic mirror; LCF, laser clean filter; NDL, 20mW 532nm Nd:YAG diode laser; DMD, digital micro-mirror device; DRC, DMD inspection camera; NF, notch filter; SP, spectrometer; CCD, charge couple device detector. The red circles in the magnified images denote the position corresponding to the focused laser on the sample, and on the sample-conjugate plane of the DMD (equivalent to zero spatial offset). (i) shows a DMD pattern for a standard confocal Raman measurement (essentially a reflective pinhole), and (ii) shows one possible SORS configuration (semi-annulus).

The CCD has an active area of 127 × 1024 (26 × 26 μm^2) pixels. The spectrograph and CCD camera were controlled by a home-built LabVIEW program. A MATLAB (MathWorks, USA) script was included in the main LabVIEW programme to allow correction of the wavenumber axis caused by shifts when the pattern of the collection points on the DMD was not vertical. After this correction, the SORS spectra corresponding to the same spatial offset could be averaged automatically.

#260530 Received 7 Mar 2016; revised 14 Apr 2016; accepted 20 Apr 2016; published 1 Jun 2016

3. Results and discussion

Concentric collection geometry for SORS with flexible offset

Conventional SORS with concentric circle input geometry is usually implemented using optical fibre bundles, where the linear arrangement at the bundle end allows the Raman spectra to be detected as separated horizontal stripes [26]. This configuration improves the collection efficiency of the Raman scattered light compared to a single point collection geometry. In this work, instead of an optical fibre bundle, we use a DMD as the offset controller for implementation of a concentric geometry collection. Figure 2(a) shows a semi-circle pattern consisting of 16 collection points displayed on the DMD. The actual size of each collection point was 30 x 30 micro-mirrors (~300 μm x 300 μm). Each point was equally distant from the point *O*, which corresponds to the conjugated point on the sample illuminated by the laser (zero spatial offset). In order to prevent crosstalk of the Raman spectra, only half of the points in the concentric circle were employed as active areas, as spectra from collection points at the same height of the DMD would be imaged to the same horizontal tracks of the CCD. For the same reason, vertical gaps of 10 micro-mirrors were included. The larger the radius of the semi-annulus (selected in the LabVIEW program), which corresponds to a larger offset distance, the more collection points were included. The actual spatial offset is calculated by the following equation:

$$\Delta x = S\frac{f_0}{f_m} \tag{1}$$

where S is the radius of semi-circle displayed on DMD, f_m and f_o are the focal lengths of the focusing lens (200 mm in this case) in front of the DMD and the focal length of the microscope objective.

For this concentric collection geometry based on a semi-circle, the area covered by the collection points (area covered by the white squares in Fig. 2(a)) represents ~25% of the total area of the annular ring (the annular area of radius $\triangle x$ represents the maximum collection area corresponding to a spatial offset $\triangle x$ – the thickness of the annulus is equal to the size of the collection points). This value compares favourably with the typical 20% reported for optical fibre bundles (26 tightly-packed collection fibres) [26]. Nevertheless, it is important to note that the signal-to-noise ratio of the Raman spectra may be limited by the optical throughput of the spectrometer, and in high-performance SORS it is common for the fibre-bundle to overfill the spectrometer slit.

However, a key advantage of the DMD-based system is the flexibility in changing the value of the offset distance, which is selected in software. The spatial offsets of conventional SORS fibre probes are fixed as the collection tracks are built into the bundle. Although inverse SORS enables an adjustable spatial offset [22], the use of an axicon optical element (i.e. a conical lens) in the laser excitation path to form laser beam rings of varying radii makes the probe design complicated. In our case, only a DMD is added in the detection path and requires no movable mechanical parts. The range of spatial offsets is determined by the dimension of DMD and the vertical number of tracks of the CCD sensor. For our system, the spatial offset can be adjusted in the 0-1 mm range when using a 2 × magnification objective (focal length 90 mm).

Figure 2(b) shows an image captured on the CCD when SORS spectra of a uniform polystyrene sample (PS) were acquired. The pattern of the peaks in the Raman spectra resembles the semi-annulus pattern displayed on the DMD (Fig. 2(a)). The stripes almost fill the entire active area of the CCD chip, limiting the spatial offset to 1 mm on the sample (Fig. 2(a)). The raw Raman spectra of the PS sample collected on the CCD are presented in Fig. 2(b) (each spectrum corresponds to vertical binning of 5 tracks on the CCD image). As each collection point of the DMD works as a reflective slit for the spectrometer, their shift in the

#260530 Received 7 Mar 2016; revised 14 Apr 2016; accepted 20 Apr 2016; published 1 Jun 2016

dispersion direction leads to spectral shifts in the measured spectra. As the shift for each collection point relative to the point of zero offset are known, all Raman spectra can be calibrated and then averaged to obtain the total Raman spectrum corresponding to the selected spatial offset. Figure 2(c) presents an example of a SORS spectrum of PS corresponding to 1 mm spatial offset (20 seconds acquisition time, 14 mW laser power).

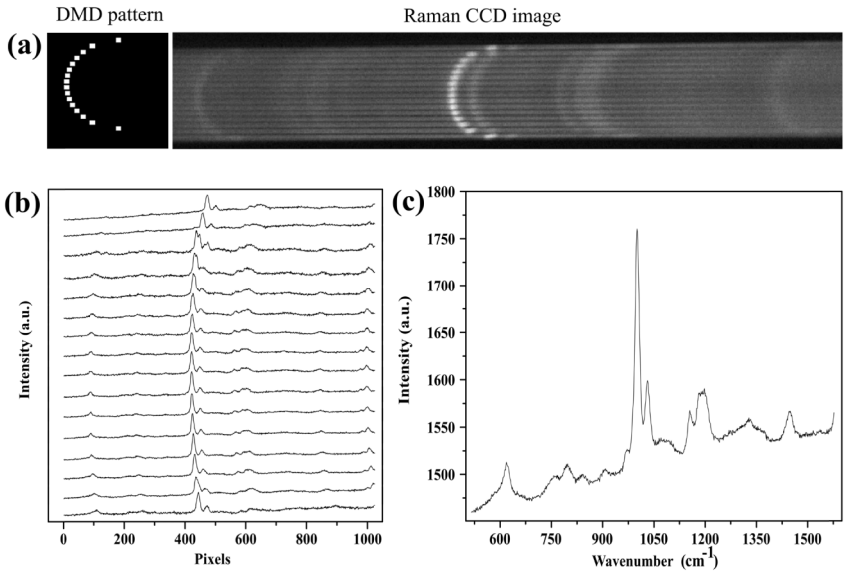

Fig. 2. (a) Semi-annulus pattern with radius of *S* displayed on DMD screen as collection zone and detection stripes imaged on the CCD camera using semi-circle collection geometry, 20s acquisition time. (b) Raman spectra of PS from the 16 collection lines shown in Fig. 2(a), each spectrum is the sum of 5 tracks. (c) The average spectrum from the measurement is shown in Fig. 2(b). The spectra are horizontally shifted to zero-offset position before averaging.

Another advantage of the DMD-based SORS instrument is the ability to vary the spectral resolution of the instrument. The resolution is determined by the size of the collection elements, which is determined by the number of micro-mirrors selected for each collection point. Thus, the spectral resolution can be adjusted by varying the number of micro-mirrors for each collection point.

The restriction of using a semi-circle pattern for the collection points applies only when Raman spectra are acquired over a broad spectral range. This avoids overlap between the spectra corresponding to the same vertical offset on the CCD. Nevertheless, for many practical applications of SORS it is common that only few selected Raman bands are used for analysis. If the spectral range is reduced such that the spectral overlapping on the CCD is avoided, then a full circular pattern of collection points can be used to in order to increase the collection efficiency. The condition for avoiding spectral overlap for the Raman spectrum on the central CCD track (track passing through the annulus centre) is:

$$\Delta\lambda \frac{dy}{d\lambda} \le \Delta x \frac{f_{sp}}{f_o} \tag{2}$$

where $\Delta\lambda$ is the spectral range of the Raman light, $dy/d\lambda$ is the linear dispersion of the spectrometer and f_{sp} is the focal length of the spectrometer. This expression can also be expressed in a simpler form as:

$$\Delta\lambda \le \Delta x \frac{a}{f_o} \tag{3}$$

#260530 Received 7 Mar 2016; revised 14 Apr 2016; accepted 20 Apr 2016; published 1 Jun 2016

where a is the grating period.

This feature is illustrated in Fig. 3, which presents SORS spectra of a PS sample after adding an optical filter blocking light outside the 555 - 565 nm range (equivalent to 779 - 1098 cm^{-1} Raman shift range at 532nm excitation). This filter ensures that only light corresponding to the two Raman peaks at 1001 cm^{-1} and 1032 cm^{-1} ($\Delta\lambda$ = 1 nm) reach the CCD detector. Considering the parameters of the instrument presented here (a = 555 nm, f_o = 90 mm), the Eq. (3) indicates that at the centre of the annulus, overlap is avoided for any spatial offsets Δx larger than 0.16 mm. These results are confirmed by the spectra presented in Fig. 3, showing no overlap for the spectra at the centre of the collection annulus when Δx = 0.3 mm (tracks 4 and 5). However, at the points near the top and bottom parts of the collection circle (e.g. tracks 2 and 3), spectral overlap is observed because the collection points corresponding to these CCD tracks on the DMD are closer.

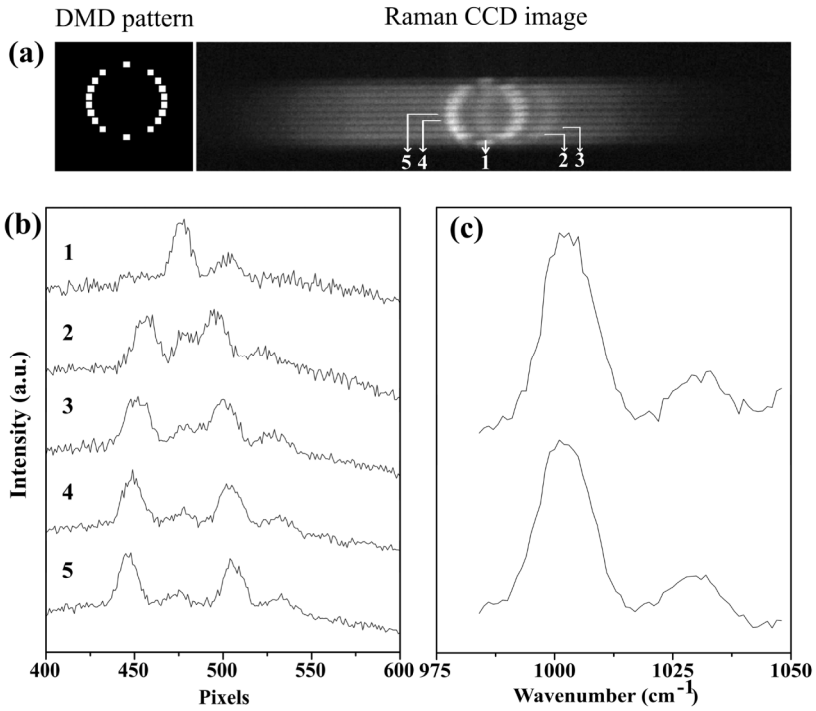

Fig. 3. (a) Full-annular collection geometry for SORS spectra and Raman spectra captured on the spectrometer CCD; (b) Raman spectra corresponding to selected rows on the CCD, as indicated by 1, 2, 3, 4, 5. (c) Mean SORS spectra obtained by averaging the spectra from semi-annular geometry (top) and full-annular geometry (bottom). Overlapped spectra, such as row 2 in (b), were excluded. Laser power: 14 mW, acquisition time 5 seconds.

Macro-SORS of two-layer samples

To demonstrate the capability and flexibility of DMD-based SORS, a two-layer structure consisting of a PMMA sheet as the top layer and PS sheet for the bottom layer was employed. Both polymer sheets are homogenous and non-transparent, with transport lengths 0.328 mm and 0.309 mm respectively (calculated from optical transmission measurements). As the light scattering parameters in the two layers are very similar, the spectral changes observed in the Raman spectra can be attributed to the sample geometry and the selection of the spatial offset values. Figure 4(b) describes the configuration geometry for the collection part for the SORS measurements, where a semi-annulus pattern of collection points was used. The SORS spectra measured for the PMMA/PS layered sample are presented in Fig. 4(c), and compared to the

#260530 Received 7 Mar 2016; revised 14 Apr 2016; accepted 20 Apr 2016; published 1 Jun 2016

Raman spectra of pure PMMA and PS. Figure 4(c) shows that the Raman band at ~809 cm^{-1} assigned to PMMA decreased gradually as the value of the spatial offset increased, while the intensity of the Raman bands assigned to PS (e.g. 1001 cm^{-1}) increase. These results show the effectiveness of SORS for recovering signals from the deeper layers of the sample, even for samples with high light scattering properties such as PS. All spectra in Fig. 4(c) were measured by simply altering the *S* parameter in the LabVIEW program controlling the DMD, without changing or adjusting any mechanical or optical elements of the instrument, highlighting the ease of use and flexible alteration of spatial offset.

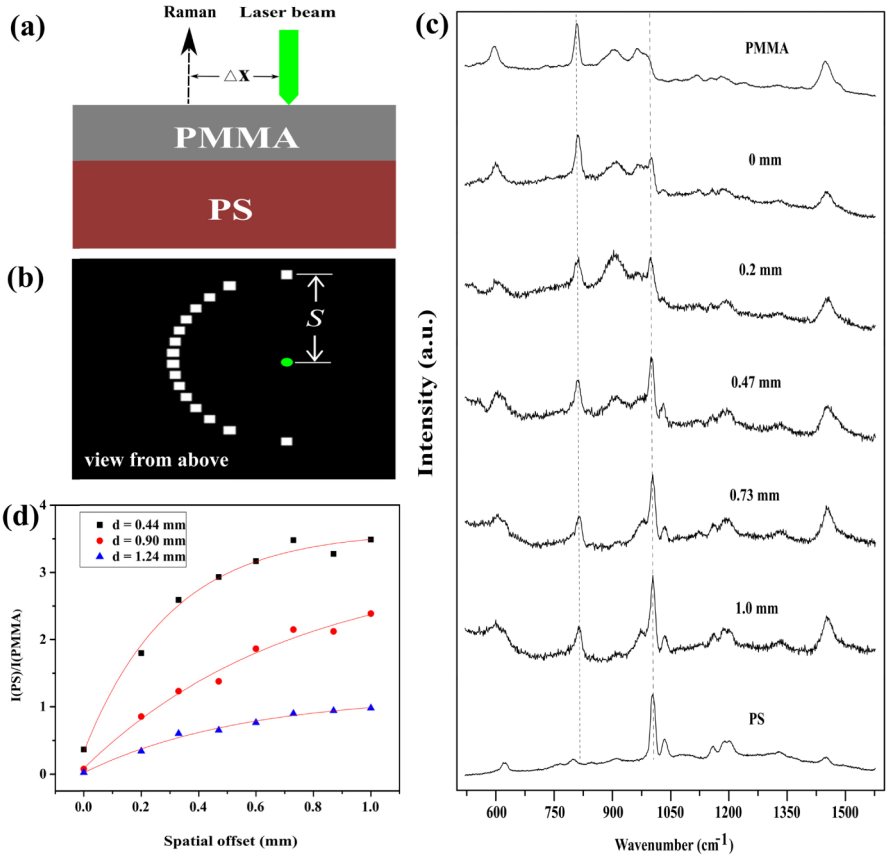

Fig. 4. (a) Schematic description of the two-layer polymer samples used in the experiment for SORS demonstration. (b) The semi-annulus collection geometry displayed on DMD and used for collection of SORS spectra. (c) A set of spatial offset Raman spectra acquired from the two-layer structure consisting of d = 0.9 mm layer of PMMA sheet and 1.0 mm of PS sheet. The acquisition time was 20 s for each spectrum. Spatial offset is indicated next to each Raman spectrum. All the spectra are shown as raw without any post processing. (d) The ratio of Raman band intensity corresponding to the bottom layer (PS) and top layer (PMMA) as a function of the spatial offset. Red eye-guiding curves are exponential fittings to the data points.

Figure 4(d) shows the dependence of the relative intensities of the Raman bands corresponding to the bottom layer (PS) to top layer (PMMA) on the spatial offset and the thickness of top layer. The data were obtained by integrating the area under the dominant Raman peak at 809 cm^{-1} for PMMA and at 1001 cm^{-1} for PS, respectively, after background subtraction. The plot shows three sets of data points calculated from measured SORS spectra from samples with PMMA thicknesses of 0.44 mm, 0.9 mm and 1.24 mm. It can be seen that the Raman intensity ratio of PS to PMMA varied as function of spatial offset, and the absolute values of the ratio are proportional to the thickness of top layer. As the spatial offset

#260530 Received 7 Mar 2016; revised 14 Apr 2016; accepted 20 Apr 2016; published 1 Jun 2016

increases, the Raman intensity ratio from the sample with thinner top layer increased more rapidly, indicating that the thicker the top layer, the more the Raman signal from bottom layer will be attenuated.

SORS measurements with simultaneous multiple offsets

The software control for the selection of the collection points for the Raman light provides the ability to measure SORS spectra for multiple spatial offsets values simultaneously. Using the two-layer sample of PMMA film (0.9 mm thickness) on a thick PS film, SORS spectra corresponding to a range of spatial offsets were collected in a single acquisition (Fig. 5). The collection geometry was modified to a V-shaped chevron pattern (Fig. 5(b)), as the points in the arm represent different spatial offsets from the point of laser incidence.

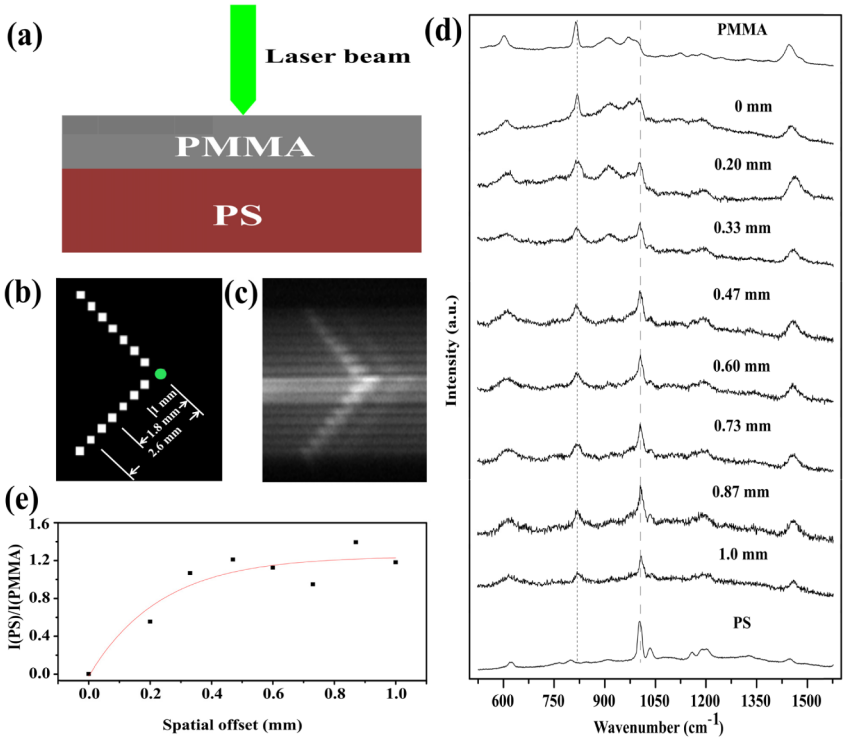

Fig. 5. (a) Two-layer sample structure of PMMA sheet and PS sheet for the multiple spatial offsets measurements. (b) The chevron pattern displayed on DMD. Each point in the arm represents a distinct spatial offset. (c) Stripes imaged on the CCD sensor using the chevron collection geometry. (d) A set of SORS spectra acquired from the two-layer polymer structure with PMMA thickness of 0.9 mm. The acquisition time was 20 s. Spatial offset is indicated next to the spectra. The spectra from pure PMMA and PS that obtained in separate measurements are also shown for comparison. (e) Ratio of Raman intensity of bottom layer (PS) to top layer (PMMA) as a function of spatial offset. Red curve is exponential fitting to the data points.

While any straight line (including a vertical line) would provide the same collection efficiency as the V-shaped arrangement, the chevron pattern allows the selection of larger spatial offset values. The points in the two arms are symmetric with respect to the horizontal line across the point corresponding to the laser spot (zero offset), so the spectrum for each spatial offset is the sum of the two spectra corresponding to the collection points in the two arms. Figure 5(c) displays the spectral stripes imaged on the CCD sensor. It can be seen again that the pattern on the CCD closely matches that of the DMD image (Fig. 5(b)). The SORS spectra (Fig. 5(d)) acquired from the two-layer polymer sample show that for the spectra

#260530 Received 7 Mar 2016; revised 14 Apr 2016; accepted 20 Apr 2016; published 1 Jun 2016

corresponding to larger offsets, the contribution of the 1001cm^{-1} Raman band corresponding to the PS substrate increases while the intensity of the 809 cm^{-1} band assigned to PMMA decreases. Under these experimental conditions, the signal to noise ratio of the spectra is lower compared to the circular collection pattern described in Figs. 3 and 4 because the collection efficiency is reduced. Nevertheless, these results demonstrate the flexibility of carrying out simultaneous SORS measurements over a broad range of offset values. Simultaneous SORS measurements with multiple offsets can be implemented in the conventional SORS setup based on fibre optic bundles by arranging the fibres in concentric annuli of different radii [26]. While the fibre bundle configuration provides better collection efficiency, the DMD-based SORS collection system allows measurements of a higher number of offsets set at smaller intervals. Furthermore, it is much simpler to switch between point, concentric and multi-offset collection geometries as the only changes required are in software. Similar to Fig. 4, the concentric circle configuration may be used in the DMD-based SORS if the spectral range is sufficiently narrow to avoid spectral overlap for the collection points of equal height.

Micro-SORS for two- and three-layer samples

Micro-SORS has been recently proposed for subsurface spectral analysis and attempting to resolve the chemical composition of thin (50 −500 μm thick) stratified layers in a sample [27–29]. There are several variants of micro-SORS, the basic principles of which have been introduced by Conti et al [30]. Defocusing micro-SORS is the most basic and easiest way to implement micro-SORS technique, as it can be readily implemented on conventional Raman microscopes without any modifications. While several studies have demonstrated that this technique can provide chemical analysis for layered samples, the interpretation of the results can be difficult because the relationship between the defocusing distance and the actual values of the spatial offset is not very clear. To overcome these difficulties and obtain improved depth-discrimination, full micro-SORS spectra can be measured by delivering the excitation laser beam to an offset point by an extra objective and collecting the Raman scattered light along the optical axis of the microscope using the microscope objective. In this case, the offset value is unambiguously defined [30]. Recent studies have indicated that this full micro-SORS provides higher relative enhancement of Raman bands corresponding to the deeper layers compared to the defocusing micro-SORS [30]. However, the implementation of full micro-SORS is difficult and the collection efficiency of the Raman signal is very low (due to the single point measurement geometry). While axicon lenses can be used to vary the spatial offset in macro-SORS, this has not been implemented in micro-SORS because of the obvious implementation difficulties.

Our DMD-based SORS instrument overcomes these difficulties as micro-SORS can be implemented as easily as macro-SORS on the same instrument by simply changing the microscope objective. Here, micro-SORS was implemented in the same Raman microscope system by simply replacing the 2 × objective used for macro-SORS with a 20 × (0.5 NA) objective for micro-SORS. The collection efficiency can be maintained above 25% by using the semi-annulus collection geometry as discussed previously (the full-annulus configuration can be used for 50% collection efficiency if the spectral range is restricted). To evaluate the instrument, we first tested the performance of the instrument when measuring SORS spectra of a two-layer sample using a thin PMMA film (200 μm thick) on a thick PS layer (1 mm). The SORS spectra obtained based on the semi-circle collection geometry are shown in Fig. 6. Figure 6(b) shows that increasing the spatial offset value leads to an increase in the intensity of the Raman bands associated to the PS substrate (e.g. at 1001 cm^{-1}) and decrease intensity of the PMMA Raman bands (809 cm^{-1}). The DMD provides unprecedented control over the values of the spatial offset values, from 15 μm to 120 μm, (with steps as small as 15 μm). Figure 6(c) presents the intensity ratio of the 1001 cm^{-1} (PS) and 809 cm^{-1} (PMMA) as a

#260530 Received 7 Mar 2016; revised 14 Apr 2016; accepted 20 Apr 2016; published 1 Jun 2016

function of spatial offset, showing the typical trend of enhancement of the signals from deeper layers of the sample when the spatial offset increases.

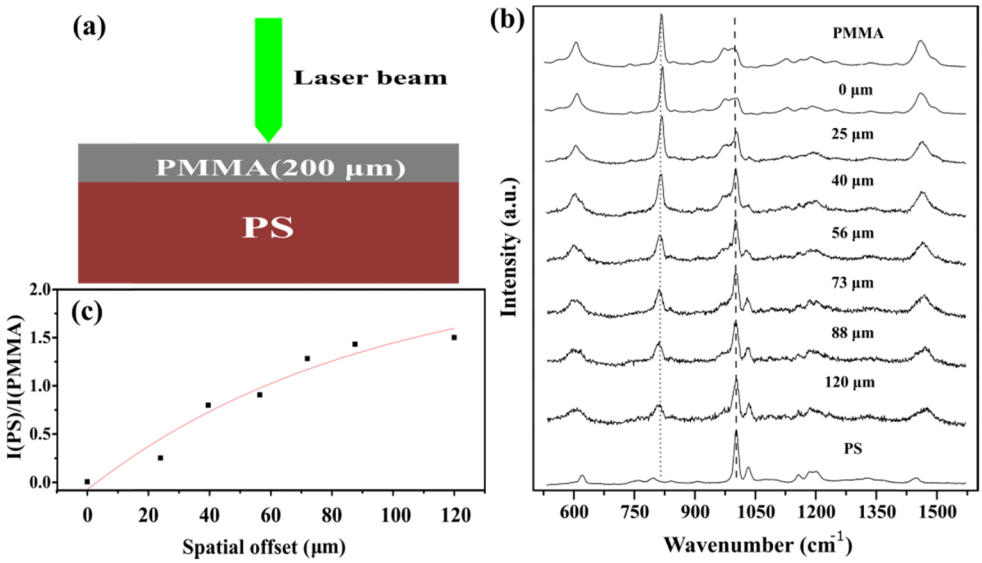

Fig. 6. (a) Two-layer sample structure of PMMA sheet and PS sheet for micro-SORS measurements. (b) Raman spectra of a two-layer sample consisting of a 200 μm thick PMMA film on thick PS substrate, acquired using the DMD-based micro-SORS system. The acquisition time was 20s for each spectrum. Reference Raman spectra from pure PS and PMMA are also displayed in the top and bottom for comparison. (c) Raman intensity ratio of PS (1001 cm^{-1}) to PMMA (809 cm^{-1}) as a function of spatial offset, calculated from the spectra shown in Fig. 6(b). The data points are fitted with exponential decay function, shown as red curve in the plot.

To demonstrate further the potential of the DMD-based SORS instrument, Fig. (7) presents micro-SORS spectra of a three-layer sample, based on a PMMA top-layer (200 μm thick), PS mid-layer (100 μm thick) and hydroxyapatite powder (HA) bottom-layer (>1 mm). The data in Fig. 7(b) shows that when the measurement is carried out with no spatial offset (confocal imaging mode), the Raman spectrum contains only bands corresponding to the PMMA top layer. As the offset is increased to 25 μm, bands at 1001 cm^{-1} and 960 cm^{-1} assigned to the PS mid-layer and HA bottom-layer begin to emerge. Further increase of the spatial offset leads to an increase in the intensity of the Raman bands associated to the PS and HA and a decrease of the bands assigned to PMMA (e.g. 809 cm^{-1}).

#260530 Received 7 Mar 2016; revised 14 Apr 2016; accepted 20 Apr 2016; published 1 Jun 2016

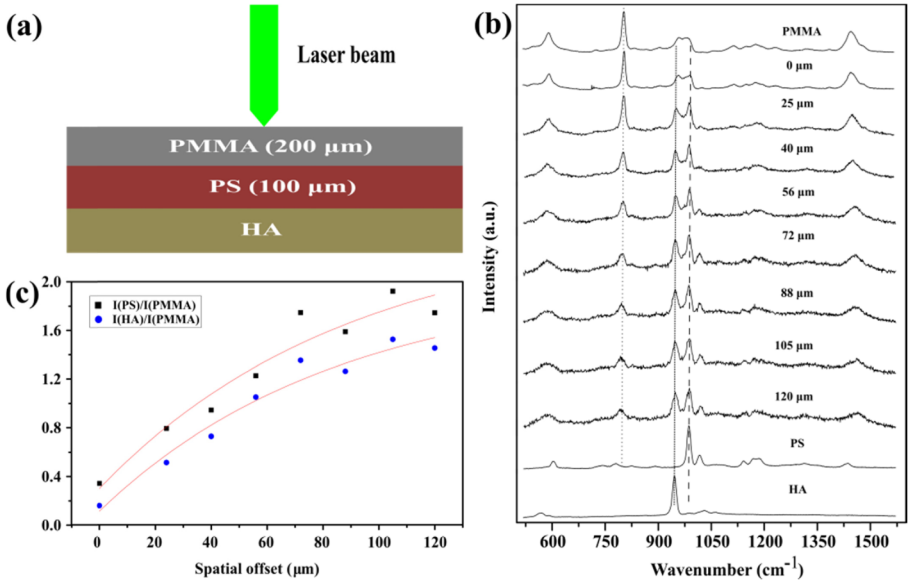

Fig. 7. (a) Schematic of a three-layer sample for micro-SORS experiment. (b) SORS spectra acquired using the semi-annulus collection geometry. The acquisition time for each spectrum was 20 s. Spatial offset is indicated next to the spectra. The spectra from pure PMMA, PS and HA (obtained in separate measurements) are also shown for comparison. (c) Raman intensity ratio of PS (1001 cm^{-1}, black squares) and HA (961 cm^{-1}, blue dots) to PMMA (809 cm^{-1}) as a function of spatial offset, calculated from the spectra shown in Fig. 7(b). The data points are fitted with exponential decay function, shown as red curves in the plot.

4. Conclusion

Macro- and micro-scale SORS have been implemented on the same Raman micro-spectrometer, facilitated by the relatively inexpensive addition of a DMD in the detection optical path. The DMD allows the system to be flexible and efficient in collecting the SORS signal using software-controllable spatial offsets, requiring no changes to the optical system or mechanical adjustment. Single-point, annular and multi-offset (chevron-shaped) collection geometries can be easily achieved by altering the pattern displayed on the DMD. These collection geometries allow high collection efficiencies for the Raman spectra (collection area as high as 50% for the full-annular configuration) or simultaneous measurements of SORS spectra at multiple offsets in a single-shot acquisition. In addition, the implementation of micro-SORS can be achieved on the same instrument by selecting a higher magnification objective. Macro- and micro-SORS measurements for two- and three-layered samples (layer thicknesses in the 100µm-1000µm range) were presented to demonstrate the potential and flexibility of the DMD-based SORS. Although this instrument has a limited range of spatial offsets (0-1 mm), this limitation is imposed by the optical microscope. In principle, the DMD can be implemented in Raman spectrometer using lenses with longer focal lengths than the microscope objectives used in this study, and optimized designs may allow a wider range of offsets.

Acknowledgments

This work was supported by the UK Engineering and Physical Sciences Research Council (grant number EP/L025620/1).

#260530 Received 7 Mar 2016; revised 14 Apr 2016; accepted 20 Apr 2016; published 1 Jun 2016